

# Lawrence Berkeley National Laboratory

## LBL Publications

### Title

Major CO<sub>2</sub> blowouts from offshore wells are strongly attenuated in water deeper than 50 m

### Permalink

<https://escholarship.org/uc/item/5t97w35h>

### Journal

Greenhouse Gases Science and Technology, 10(1)

### ISSN

2152-3878

### Authors

Oldenburg, Curtis M  
Pan, Lehua

### Publication Date

2020-02-01

### DOI

10.1002/ghg.1943

Peer reviewed

Major CO<sub>2</sub> blowouts from offshore wells are strongly attenuated in  
water deeper than 50 m

Curtis M. Oldenburg

Lehua Pan

Energy Geosciences Division

Lawrence Berkeley National Laboratory

Berkeley, CA 94720

November 20, 2019

Keywords: CO<sub>2</sub> well blowout, wellbore modeling, offshore well blowout, buoyant plume, integral plume model, CO<sub>2</sub> in water column

### **Abstract**

Growing interest in offshore geologic carbon sequestration (GCS) motivates evaluation of the consequences of subsea CO<sub>2</sub> well blowouts. We have simulated a hypothetical major CO<sub>2</sub> well blowout in shallow water of the Texas Gulf Coast. We use a coupled reservoir-well model (T2Well) to simulate the subsea blowout flow rate for input to an integral model (TAMOC) for modeling CO<sub>2</sub> transport in the water column. Bubble sizes are estimated for the blowout scenario for input to TAMOC. Results suggest that a major CO<sub>2</sub> blowout in  $\geq 50$  m of water will be almost entirely attenuated by the water column due to CO<sub>2</sub> dissolution into seawater during upward rise. In contrast, the same blowout in 10 m of water will hardly be attenuated at all. Results also show that the size of the orifice of the leak strongly controls the CO<sub>2</sub> blowout rate.

### **Introduction**

Interest in offshore continental shelf regions for geologic carbon sequestration (GCS) is growing in the U.S. and elsewhere, and with that comes the need to understand consequences of very rare and unexpected high-flow-rate carbon dioxide (CO<sub>2</sub>) well blowouts and pipeline ruptures. Such failures of containment were addressed in the 2005 IPCC Special Report<sup>1</sup>, but killing well blowouts was reported then to be routine and effective, contrasting with the recent experiences

with two well-known hydrocarbon well blowouts, the 2010 Deepwater Horizon<sup>2</sup> and 2015 Aliso Canyon incidents<sup>3</sup>, both of which took several months to plug. Although there is no explosion or flammability hazard associated with pure CO<sub>2</sub>, there are health and safety hazards of high CO<sub>2</sub> concentrations in air associated with inhalation that could result from CO<sub>2</sub> bubbling to the sea surface. But in the offshore environment, the risk to humans is inherently lower relative to most onshore scenarios because the population at risk is limited to the few people on boats, ships, and platforms. Nevertheless, it is necessary to quantify the behavior and potential consequences of major CO<sub>2</sub> blowouts and pipeline ruptures originating at the seafloor, particularly in shallow water (water column < 150 m (500 ft)). For example, in order to assess the risk of major CO<sub>2</sub> blowouts we need to know whether the blowout will cause CO<sub>2</sub> surface emissions and create a sea-surface-hugging atmospheric CO<sub>2</sub> plume that is hazardous to people and marine life, or create a geyser-like emission, or bubbly and turbulent sea surface causing instability for boats and ships. Or maybe the CO<sub>2</sub> will mostly dissolve in the water column rendering the blowout harmless to boaters and platform personnel. And we need to know to what degree factors such as water depth and blowout flow rate affect attenuation of leaking CO<sub>2</sub> by the water column.

To answer these questions and more, we have simulated a hypothetical major CO<sub>2</sub> blowout from a deep CO<sub>2</sub> injection well-pipeline system and used the output from that simulation as input to a second model to analyze the processes of flow and attenuation of the buoyant CO<sub>2</sub> plume in the water column. The study parallels in some ways the study by Xinhong et al.<sup>4</sup> on natural gas releases from subsea pipelines. The main difference is that we examine CO<sub>2</sub> transport in the water column and our source term comes from CO<sub>2</sub> flow up a well connected to a GCS reservoir rather than a pipeline. The scenario we consider represents a very rare blowout incident at a prototypical future near-offshore (shallow water) CO<sub>2</sub> storage site with reservoir, well, and water column regions as shown in Figure 1. The essential processes depicted for a blowout in Figure 1 are two-phase porous media flow in the reservoir with decompression as the fluids (supercritical CO<sub>2</sub> and aqueous brine) flow toward the well, and then two/three-phase (aqueous, gas, and liquid CO<sub>2</sub>) flow up the well with strong decompression due to the long vertical travel distance. Near the top of the well (10 m from the wellhead) in our scenario is a hole in the pipe connected to the well out of which the fluids flow with strong decompression into the water column. The main processes in the water column just above the leakage point are jet flow of CO<sub>2</sub> out of a small orifice (hole) that we vary in size as part of the study, the turbulent instability at the interface between the jet and the ambient seawater, the formation of bubbles mixed in with seawater arising from this turbulence, and the entrainment of seawater into the CO<sub>2</sub> plume. As momentum is lost from the plume to the ambient seawater, bubbles of various sizes form and the CO<sub>2</sub> plume then becomes a buoyant plume subject to dissolution into the seawater as it rises upward. Whatever CO<sub>2</sub> does not dissolve in the water column is then emitted into the atmosphere where ambient winds and density-driven flow act to transport and disperse the CO<sub>2</sub>. In this study, our focus is on the subsurface and water column processes and we do not report here on atmospheric dispersion or its modeling.

We emphasize that this initial modeling effort was carried out to aid understanding of the general processes and sensitivities of shallow offshore subsea CO<sub>2</sub> well blowouts into the water column. The model scenario is idealized and site- or scenario-specific factors should be taken into consideration before applying the results to any particular site risk assessment. Furthermore, the simulation results are focused on the first-order question related to human health risk assessment, namely, to what degree does the water column attenuate the CO<sub>2</sub> so it is not emitted at the sea surface, rather than more subtle aspects of environmental risk assessment and monitoring of offshore GCS that have been studied previously<sup>5,6,7</sup>.

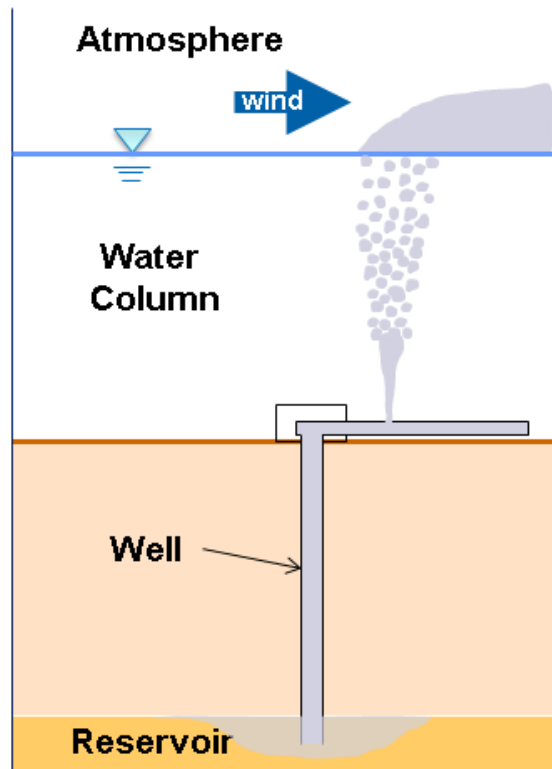


*Figure 1. Conceptual model of an offshore CO<sub>2</sub> well with blowout near the wellhead showing the reservoir, well, short pipe segment, water column, and atmospheric regions.*

## **Background**

### ***1. Motivation***

Wells are widely recognized as potential leakage pathways for CO<sub>2</sub> and other fluids at GCS sites<sup>8</sup>. Most studies of well leakage into the atmosphere in the GCS context focus on the question of whether GCS is an effective long-term mitigation for CO<sub>2</sub> emissions, and particularly on low leakage rates from large numbers of abandoned onshore oil and gas wells<sup>9</sup>. However, localized leakage from a single well blowout or a few wells at GCS sites can cause health and safety hazards especially for localized high-flow-rate incidents (i.e., high CO<sub>2</sub> leakage flux). Note that while the term “blowout” in the oil and gas context is defined as any uncontrolled leakage of fluids, a major blowout is usually understood to imply large flow rates (> 10 kg/s) from a localized leakage pathway up a well<sup>10</sup>. For pipeline failure resulting in a large leakage flow rate, the term “rupture” is used with a major rupture having flow rates larger than 10 kg/s<sup>10</sup>. Although the scenario we examine here involves CO<sub>2</sub> leaking from a hole in a pipe next to the well (10 m away), we refer hereafter to the leak as being a well blowout because the source of CO<sub>2</sub> is the reservoir (connected via the well) rather than the pipeline which we assume would be immediately shut off following the detection of the leak.

### ***2. Prior Work***

Statistics of onshore well blowout incidents and associated risk perception, including blowouts from steam injection wells, have been analyzed as a way of inferring blowout risk for a future widespread implementation of onshore GCS<sup>11,12</sup>. Maps of near-offshore oil and gas fields in the Gulf of Mexico and elsewhere show very high densities of old wells subject to potential individual and collective leakage including blowouts<sup>13</sup>. As part of evaluating the GCS potential of the offshore Gulf of Mexico region, it is necessary to evaluate the consequences of potential major CO<sub>2</sub> well blowouts. We note that near-offshore GCS will also involve subsea CO<sub>2</sub> pipelines and distribution lines that are also subject to non-zero failure likelihood and whose ruptures would result in major CO<sub>2</sub> flows into the water column very similar to well blowouts, although they would likely be short-lived as the pipeline would be shutdown after detection of the leak. In contrast, well blowouts can be very difficult to kill and can flow for months or more before being killed and plugged.

Literature on major CO<sub>2</sub> well blowouts that can serve as analogues for GCS CO<sub>2</sub> well blowouts is scarce even though CO<sub>2</sub> has been produced from natural onshore CO<sub>2</sub> accumulations (domes) for enhanced oil recovery (CO<sub>2</sub>-EOR) since the early 1970's<sup>14</sup>. One exception is the Sheep Mountain CO<sub>2</sub> production facility well blowout thoroughly described by Lynch et al.<sup>15</sup>. And well blowouts are known to occur during CO<sub>2</sub> injection for enhanced oil recovery<sup>16</sup>. In the area of offshore GCS feasibility and risk assessment, the evaluation of impacts of minor (0.1 – 1 kg/s) and medium (1 – 10 kg/s) leakage rates over large areas is a very active research area<sup>17,18,19</sup>. A hypothetical major CO<sub>2</sub> blowout scenario in the North Sea was evaluated for its impacts on ocean acidification and large-scale dissolved CO<sub>2</sub> circulation rather than on the details of ebullition, dissolution, or emission at the sea surface<sup>20</sup>. We have previously carried out high-

flow-rate single-well CO<sub>2</sub> blowout simulations for onshore and offshore wells<sup>21,22</sup> without analysis of attenuation by the water column. Researchers at Sintef (Norway) have developed and demonstrated a sophisticated computational fluid dynamics (CFD) simulator of gas blowouts into the water column applicable to major CO<sub>2</sub> blowouts<sup>23</sup>. Sintef researchers have also written a comprehensive summary of the state of understanding of offshore gas release that covers both natural gas and CO<sub>2</sub> systems<sup>10</sup>.

The largest contributions to the science and technology of offshore well blowouts and pipeline ruptures come from the experiences with producing oil and natural gas including laboratory experiments of gas-release processes<sup>24</sup>. The vast amount of literature related to offshore oil and gas well blowouts includes the development, application, and comparison of simulation tools and models for oil and natural gas fate and transport in the water column often for deep-water (> 150 m (500 ft) depth) environments<sup>25,26,27,28,29,30</sup>. The tools developed for simulating high flow-rate natural gas and oil releases are generally applicable to CO<sub>2</sub> releases provided an option exists to use an equation of state for CO<sub>2</sub> as an alternative to natural gas and oil. One such model with this capability is the Texas A&M oil spill (outfall) calculator (TAMOC)<sup>31,32,33,34</sup>, which we use in this study.

### ***3. Caveats Relevant to Analogues***

Although the nicely documented Sheep Mountain Dome CO<sub>2</sub> well blowout<sup>15</sup> serves as a useful analogue for GCS well blowouts, it is important to mention some differences between natural accumulations of CO<sub>2</sub>, and natural accumulations of oil and gas for that matter, versus CO<sub>2</sub> injected into GCS storage reservoirs. First, natural accumulations of CO<sub>2</sub> or oil and gas can be over-pressured in the reservoir relative to hydrostatic conditions by various geologic processes (erosion of overlying formations, unloading of the crust by glacial ice melting, etc.), whereas GCS reservoirs will most likely be at hydrostatic conditions or slightly above with CO<sub>2</sub> injection pressure carefully controlled to avoid fracturing and to minimize pressure rise in the reservoir. Second, natural accumulations have had millions of years to stabilize under gravity and capillary forces. In contrast, GCS reservoirs in the near future will still be undergoing active injection of CO<sub>2</sub> with highest CO<sub>2</sub> saturations near the well and CO<sub>2</sub> plume front migrating outward variable distances depending on how long injection has been occurring. An oil and/or gas well that suffers loss of containment failure at the wellhead (or nearby in a pipeline) and is perforated in the “pay zone” might be expected to tap a large volume of naturally occurring mobile hydrocarbon phase(s) while a similar GCS CO<sub>2</sub> injection well blowout taps the fraction of CO<sub>2</sub> that is not capillary trapped<sup>35</sup> and likely not the CO<sub>2</sub> in the far-field that is migrating under gravity-capillary forces<sup>36</sup>.

As for processes occurring in the well, oil will exsolve large amounts of natural gas as it decompresses in flowing up the well. The main analogue of this process in a CO<sub>2</sub> well undergoing a major blowout is that reservoir brine flowing up the well will degas CO<sub>2</sub>, with the total amount of gas exsolving being low relative to natural gas exsolving from oil due to the relatively low CO<sub>2</sub> solubility in brine. For all three well types, oil, dry gas, and CO<sub>2</sub>, the low

density of the fluids filling the well does not balance against the much higher (approximately hydrostatic) pressure at the bottom of the well, a situation that creates the strong underpressure in the well and driving force for the blowout. On the other hand, the density of CO<sub>2</sub> is much larger than that of natural gas, and one study found that if the 2015 Aliso Canyon incident had occurred in a GCS reservoir instead of a natural gas storage reservoir, the volumetric flow rate of gas (CO<sub>2</sub>) would have been approximately 25% of the flow rate of natural gas that actually occurred, with correspondingly smaller pressure at the discharge point likely making well-killing easier<sup>37</sup>. Oil well blowouts can be expected to have three phases (oil, gas, and aqueous) whereas CO<sub>2</sub> wells or dry gas wells will normally have two phases (gas/supercritical and aqueous) unless severe decompression cooling is occurring, in which case oil and gas and CO<sub>2</sub> wells would also have solid phase(s) (hydrates and/or water ice), along with liquid CO<sub>2</sub> (in the case of the CO<sub>2</sub> well) as additional possible phases. Killing major blowouts can be very challenging because there is no single failure mode, no single leakage flow path, and no single reservoir nor fluid composition. Each case is different and well-blowout professionals often need to try multiple approaches before successfully killing blowouts. In two major recent incidents, the 2010 Macondo well blowout and the 2015 Aliso Canyon well blowout, top-kills were unsuccessful and the two wells flowed uncontrolled for approximately three months while relief wells were drilled so that bottom kills could be used to ultimately kill and plug the wells<sup>2,3</sup>.

In summary, although there are significant differences between oil and gas reservoirs, natural CO<sub>2</sub> domes, and CO<sub>2</sub> storage reservoirs as outlined above, and every reservoir will have its own characteristics of flow and fluid properties that influence flow characteristics of a major blowout, there are also broad similarities that make experience with one relevant to the others: (1) wells in all four cases are designed either for high productivity or high injectivity and as such are perforated in high transmissivity zones that can tap large amounts of buoyant fluids; (2) blowouts tend to be self-sustaining because hydrocarbons and CO<sub>2</sub> have lower density than water leading to a well column that is strongly under-pressured relative to the reservoir pressure; and (3) blowouts can be very challenging to kill.

## **Processes and Methods**

### ***1. Overview***

The main goal of this study was to model CO<sub>2</sub> transport processes in the water column to understand attenuation processes and the controls on CO<sub>2</sub> transport following a major CO<sub>2</sub> well blowout. To obtain the inputs for the water-column part of the model, we simulated a prototypical major CO<sub>2</sub> well blowout using T2Well which couples well and reservoir flows<sup>38,39,40</sup>. Specifically, T2Well couples two-phase Darcy flow in the subsurface reservoir with two-phase pipe flow in the well modeled by the drift-flux model. This approach has been demonstrated previously including for an onshore CO<sub>2</sub> well blowout<sup>21</sup>, for the Macondo oil and gas blowout<sup>41</sup>, and for the Aliso Canyon natural gas blowout<sup>42</sup>. The recent interest in offshore GCS led us to a study comparing onshore to offshore well blowouts, in which we concluded that

the main differences between onshore and offshore well blowouts arise because of CO<sub>2</sub> transport processes in the water column that are absent in onshore scenarios<sup>22</sup>.

## **2. Water-Column Modeling**

With the focus on the water column part of the system, we note that relative to ambient air in an onshore scenario, the water column provides

- Strong inertial resistance to flow initially for CO<sub>2</sub> first entering the water column
- Viscous resistance, turbulent seawater entrainment, and surface tension leading to CO<sub>2</sub> bubble formation
- Positive buoyancy for CO<sub>2</sub> instead of negative buoyancy
- Vast source of heat to counter expansion cooling during upward transport
- Vast sink for CO<sub>2</sub> dissolution during upward transport

In order to understand the CO<sub>2</sub> transport processes in the water column following a major blowout, we use the TAMOC model with inputs supplied by the output of T2Well. TAMOC is a multipurpose modeling suite for multiphase offshore oil and gas spill simulations, natural gas underwater releases, and single-phase plumes. TAMOC includes capabilities to model major blowouts or ruptures and the transition to a buoyant bubble or droplet plume as entrainment and ebullition occur<sup>31,34</sup>. For our purposes of modeling a CO<sub>2</sub> well blowout, we make use of TAMOC's built-in equation of state model<sup>32</sup> and the default TAMOC database including CO<sub>2</sub> chemical properties that extends TAMOC's applicability to CO<sub>2</sub> blowouts<sup>43</sup>. We further chose to use the bent-plume model (BPM) that handles the case of a buoyant CO<sub>2</sub> plume moving in ambient seawater with a nominal overall cross current. TAMOC uses an integral approach to model the buoyant bubble plume and entrained sea water<sup>44,45,34</sup> and models the dissolution processes by a discrete particle model<sup>46,47</sup>. Integral approaches are simple, robust, and computationally efficient and have been used for decades in both single and multiphase contexts<sup>48,49,50</sup>. TAMOC has been extensively tested and validated on both laboratory and field measurements of various kinds of fluid and gas releases<sup>34,32,33,19,51</sup>. Inputs to TAMOC include the CO<sub>2</sub> leakage rate, the diameter of the orifice out of which the CO<sub>2</sub> is leaking, the water depth, temperature, and salinity of the seawater at the leak point, the temperature and salinity profiles in the water column, and the background large-scale cross current in the water column. As an integral model, TAMOC simulates the behaviors of various size classes of bubbles rather than individual bubbles, therefore inputs on bubble size and bubble-size distribution are required<sup>34,52</sup>.

## **3. Initial Bubble Size and Distribution**

The starting point for modeling CO<sub>2</sub> transport in the water column of a major blowout using TAMOC is the estimate of the initial bubble sizes and their distribution starting at the point where the CO<sub>2</sub> jet begins transitioning to a buoyant bubble plume. Input to this workflow comes from the output of T2Well which consists of the mass flow rate, pressure, temperature, and CO<sub>2</sub> density at the point of leakage, e.g., just upstream of the leakage source (orifice or hole). From this T2Well output, the velocity of the leaking CO<sub>2</sub> ( $u_g$ ) can be calculated. The key length scale

over which ebullition occurs is the distance ( $l_M$ ) over which the kinematic (inertial) momentum flux transitions to buoyant momentum flux, a length scale referred to as the penetration length of the jet. The approach to bubble-size estimation that we follow is based on a combination of scaling laws and empirical results<sup>52</sup>. Here we briefly summarize the workflow assuming that the leakage is all CO<sub>2</sub> which makes mixture properties equal to gas properties, e.g., the area of the leaking mixture is the same as the area of the leaking gas, and the density of the mixture is the same as the density of the gas ( $A = A_g$ , and  $\rho_m = \rho_g$ ), etc. Full details and background on these methods can be found in Dissayanake et al.<sup>34</sup> and as modified by Wang et al.<sup>52</sup> based on experimental data.

By the assumption that the leaking fluid is all CO<sub>2</sub> (e.g., no oil and no water), the kinematic momentum flux is given by

$$m_0 = \rho_g A_g u_g^2 \quad (1)$$

and the buoyancy flux is given by

$$b_0 = (\rho_a - \rho_g) g A_g u_g = (\rho_a - \rho_g) g u_g \frac{D^2 \pi}{4} \quad (2)$$

(see Nomenclature for definition of symbols). Normalizing these kinematic and buoyancy flux terms by the ambient seawater density, we obtain kinematic momentum and buoyancy terms as follows:

$$M = \frac{m_0}{\rho_a} \quad (3)$$

$$B = \frac{b_0}{\rho_a} \quad (4)$$

From these terms, the penetration length scale of the jet is given by the scaling relation<sup>52</sup>

$$l_M = \frac{M^{3/4}}{B^{1/2}} \quad (5)$$

The Weber number ( $We_m$ ) is the ratio of kinematic momentum to surface tension known to characterize turbulent bubble breakup and formation. Because ebullition occurs within the transition from jet to buoyant plume regions,  $We_m$  requires a velocity scale that includes both jet and ambient fluid velocity characteristics. Wang et al.<sup>52</sup> defined an ambient fluid velocity for the Weber number that can be written as follows assuming single-phase gas release:

$$U_a = \sqrt{\frac{m_0}{\rho_a A}} = \sqrt{\frac{\rho_g A_g u_g^2}{\rho_a A}} = \sqrt{\frac{\rho_g A_g u_g^2}{\rho_a} \frac{4}{D^2 \pi}} = u_g \sqrt{\frac{\rho_g}{\rho_a}} \quad (6)$$

The Weber number is then given by

$$We_m = \frac{U_a^2 l_M \rho_m}{\sigma} \quad (7)$$

where in this case  $\rho_m$  is  $\rho_g$  because we assume a single-phase gas blowout (no aqueous phase). Experiments by Wang et al.<sup>52</sup> showed their data fit the following equation for the mean bubble size:

$$d_{50} = l_M 4.3 We_m^{-3/5} \quad (8)$$

The distribution of bubble sizes has been shown empirically to fit the Rosin-Rammler cumulative volume distribution given by

$$V(d) = 1 - \exp \left[ -k_{50} \left( \frac{d}{d_{50}} \right)^\alpha \right] \quad (9)$$

where  $k_{50} = 0.693$  and  $\alpha = 5.2$ <sup>52</sup>.

The bubble sizes and their distribution are important for controlling the rate of bubble dissolution. Specifically, in the discrete particle model, the mass of component  $i$  ( $m_i$ ) in the bubble changes with time proportional to the product of the surface area of the bubble ( $A_b$ , (m<sup>2</sup>)), the mass transfer coefficient ( $\beta_i$  (m/s)), and the difference in the seawater aqueous concentration of  $i$  (mass per volume) adjacent to the bubble ( $C_{s,i}$ ) and the equilibrium aqueous concentration of  $i$  in the ambient seawater ( $C_i^{eq}$ ) by the equation

$$\frac{dm_i}{dt} = -A_b \beta_i (C_{s,i} - C_i^{eq}) \quad (10)$$

A sketch of a single bubble showing the parameters of Eq. 10 is presented in Figure 2. The concentration of component  $i$  just outside the bubble wall,  $C_{s,i}$ , can be approximated by the solubility of component  $i$  in seawater<sup>34</sup>.  $C_i^{eq}$  is calculated in our TAMOC simulations as the concentration that results from dissolution of the bubbles in the volume of water containing the bubble plume<sup>19</sup>. In other words, the equilibrium seawater concentration of component  $i$  rises as bubbles dissolve, thereby decreasing the concentration gradient driving mass transfer. With bubble area explicit in Eq. 10 and volume implicit in the mass term, the bubble surface area to volume ratio is a strong control on dissolution rate, with bubbles ten times smaller in diameter dissolving ten times faster, all other things being equal.

The mass transfer coefficient ( $\beta_i$ ) also controls bubble dissolution rate, and its value is reduced by contaminants that accumulate on the gas-water (bubble) interface. In this study, we assume that the interface is contaminated (so-called dirty bubble assumption) resulting in smaller assumed values of  $\beta_i$  relative to those for uncontaminated (clean bubble) interfaces. The mass transfer coefficient is calculated in TAMOC for the conditions of the CO<sub>2</sub> blowout case considered here by the correlations of Clift et al.<sup>53</sup> (Table 5.4, p. 123) resulting in a mass transfer coefficient of approximately  $1 \times 10^{-4}$  m/s for the median bubble-size (0.5 mm, see *Results Section 2*), in excellent agreement with other correlation summaries for dirty bubbles<sup>54</sup>. This mass transfer coefficient is only weakly dependent on bubble size for the blowout release conditions considered here, decreasing by about 20% as bubble size increases over its range from 0.1 to 1 mm (see *Results Section 2*). A brief discussion of bubble-to-seawater mass transfer in Eq. 10 and as observed in the simulations is given in the *Conclusions and Discussion* section.

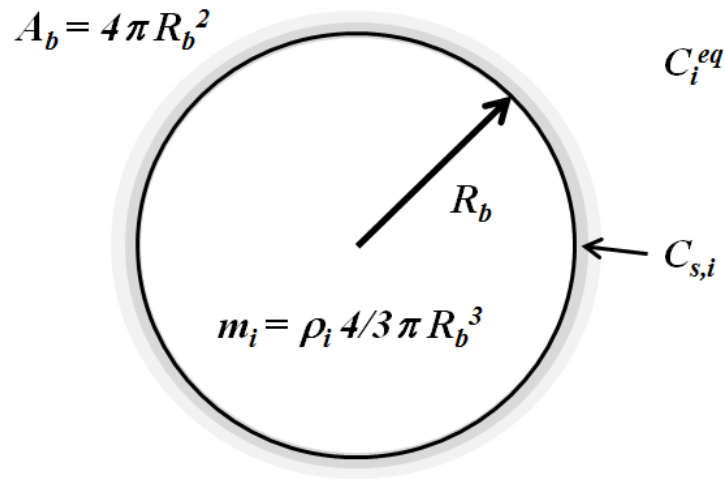


Figure 2. Two-dimensional cross section of a spherical bubble illustrating the variables of Eq. 10 that control mass transfer in the discrete particle model.

### 3. Well Blowout Modeling

We assume CO<sub>2</sub> injection is occurring in a well perforated at a depth of 3000 m with a seabed wellhead at a temperature of 22.78 °C and various hydrostatic pressures depending on water column height (depth). The tubing of the well is assumed to be connected to a pipe (flowline) on the seafloor that ruptures due to a nominally 2 inch- (0.0508 m-) diameter hole.<sup>1</sup> Upon rupture, the upstream pipeline is assumed to be shut-in (no flow) while the reservoir pressure drives the well blowout. Sketches of the model system and details of the well are shown in Figure 3. Properties of the well and reservoir systems are given in Tables 1 and 2. The values chosen for the various dimensions and properties of the system are representative of a large-scale offshore saline GCS project.

Briefly, the reservoir consists of a 50 m-thick sandstone with 90% CO<sub>2</sub> saturation as might occur following many years of CO<sub>2</sub> injection for GCS. Capillary pressure and relative permeability parameters are shown in Table 2. Because the reservoir is assumed to be hydrostatic and connected hydraulically to the seafloor, the initial effective pressure difference is 29.43 MPa for all of the various cases of varying water column height (depth). Meanwhile reservoir temperature is the same for all the various depth cases. At  $t = 0$ , the well tubing is assumed to be filled with CO<sub>2</sub> in gas-static equilibrium with the reservoir pressure, and the well is closed except for the 2-inch hole 10 m from the wellhead at which point the  $P$ - $T$  conditions are 0.598 MPa (50 m depth offshore case) and 22.78 °C.

The well exchanges heat with the surrounding formations by conduction calculated using the analytical approach embedded in T2Well<sup>38,56</sup>. Heat exchange between the surface pipe and the surrounding seawater is simulated numerically by thermally connecting grid cells to a constant temperature grid cell with given thickness of the pipe wall (1.072 cm) and thermal conductivity of steel (55 W/(m °C)).

---

<sup>1</sup> Note that formally what is specified in T2Well is that the hole has an area of 2.0268E-3 m<sup>2</sup> and a perimeter of 0.33163 which corresponds to a crack approximately six-inches long by 0.6 inches across. The nominal diameter 0.0508 comes from assuming that the crack is circular ( $D = 2 \times \text{SQRT}(2.0268\text{E-}3/\pi) = 0.0508$  m).

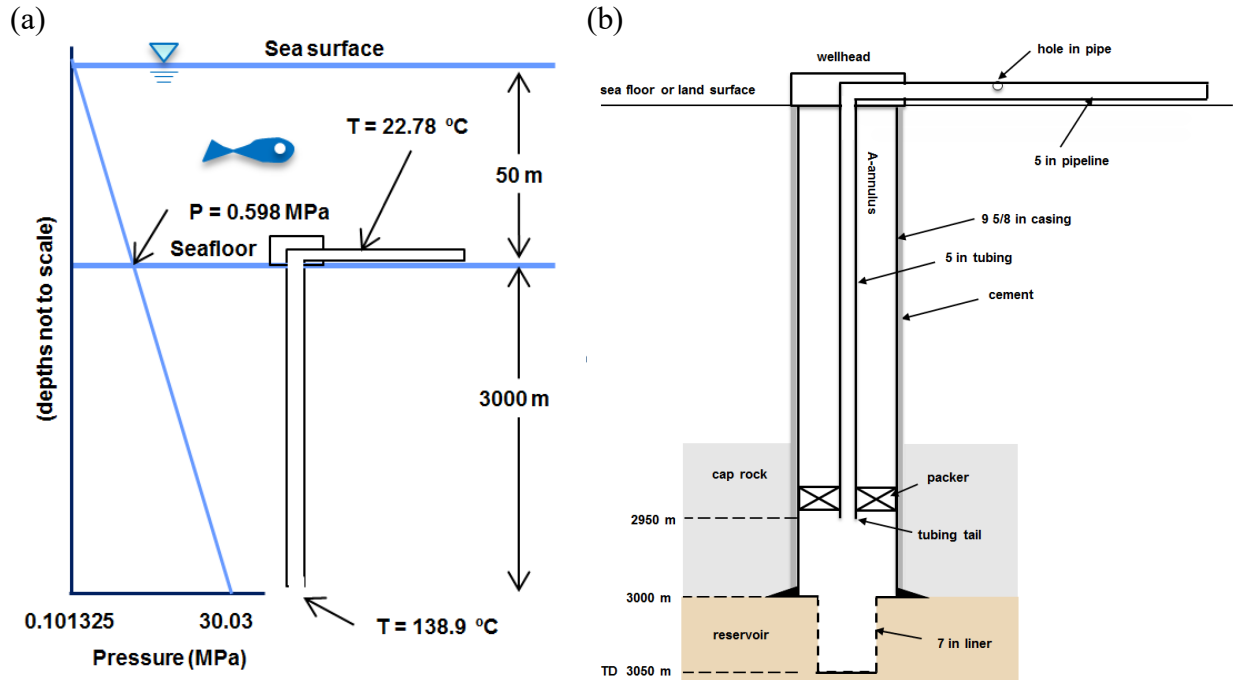


Figure 3. (a) Sketch of pressure, temperature, and depth conditions for the 50 m-deep offshore well, and (b) reservoir and well system domain used in the T2Well blowout simulation.

Table 1. Representative dimensions of the components of a CO<sub>2</sub> injection well assumed for the well in this study..

Model element	Value
Seafloor pipe	ID = 0.10556 m (5 inch tubing), horizontal, with hole located 10 m away from the wellhead
Tubing	ID = 0.10556 m (5 inch tubing), vertical, (0-2900 m)
Casing	ID = 0.2205 m (9 5/8 inch casing, 0 – 3000 m, simulated 2900-3000 m)
Liner	ID = 0.15037 (7 inch liner, 3000-3050 m from seafloor, perforated)
Break in pipe (hole in pipe)	Effective ID = 0.0508 m (2 in) (10 m away from the center of well)
Tubing and pipeline wall roughness	$45.72 \times 10^{-6}$ m

Table 2. Representative prototypical reservoir properties assumed for the storage reservoir.

Reservoir Properties	
Thickness	50 m
Depth of lowermost cap rock	3000 m
Porosity ( $\phi$ )	0.20
Permeability ( $k$ )	$1.0 \times 10^{-12} \text{ m}^2$
Compressibility of reservoir formation	$8.5 \times 10^{-10} \text{ Pa}^{-1}$
Thermal conductivity of reservoir saturated reservoir formation	2.50 W/(m K)
Heat capacity ( $C_p$ ) of saturated reservoir	1000 J/(kg K)
Capillary Pressure ( $P_{cap}$ ) and Relative Permeability ( $k_r$ ) <i>Terminology:</i> $m = 1-1/n$ = power in expressions for $P_{cap}$ and $k_r$ $S_{ar}$ = aqueous-phase residual saturation $S_{gr}$ = gas-phase residual saturation $P_{c0}$ = capillary pressure strength between aqueous and gas phases $P_{cmax}$ = maximum possible value of $P_{cap}$	van Genuchten <sup>55</sup> $P_c$ and $k_r$ with Corey <sup>57</sup> relative permeability for gas  $m_{vG} = 0.457$ $S_{ar} = 0.30$ for $P_{cap}$ , 0.36 for $k_r$ $S_{gr} = 0.05$ $P_{c0} = 1.25 \times 10^4 \text{ Pa}$ $P_{cmax} = 1 \times 10^7 \text{ Pa}$
Initial pressure	30.03 MPa in 50 m depth case
Initial temperature	138.9 C Geothermal gradient 38.39 C/km Offshore seafloor $T = 22.78 \text{ }^\circ\text{C}$
Initial saturation	0.1 aqueous saturation; 0.90 CO <sub>2</sub> saturation

T2Well simulates transient multiphase flow in the wellbore using the drift-flux model (DFM) coupled with porous media (Darcy) flow in the reservoir through well-reservoir connections at the perforations<sup>39</sup>. The CO<sub>2</sub>-water properties are modeled using a research version of ECO2N/ECO2M<sup>40,42</sup> that handles CO<sub>2</sub> phase change and low temperatures that can arise during CO<sub>2</sub> blowouts involving gaseous, liquid, and supercritical phases of CO<sub>2</sub> along with saline water. We use a radial 1D grid for the reservoir (50 m thickness,  $\Delta R$  varies from 0.03 m to 200 m at far field of  $\sim 1$  km), and a 1D grid for the well (50 m vertical resolution) plus a 1D grid for surface pipe (10 grid cells).

## Results

### 1. Well blowout

As shown in Figure 4 for the 50 m and 10 m depth cases, the initial CO<sub>2</sub> release is a two-phase mixture of liquid and gaseous CO<sub>2</sub> that quickly (after approximately 6 and 30 minutes,

respectively) changes to be all gas with a steady flow rate of approximately 36 kg/s. Note that there is a small amount of aqueous phase that condenses from the CO<sub>2</sub>. This small amount of water is negligible and was neglected in the water column transport modeling considered next. Figure 4b shows the temperatures at the wellhead and at the hole (leak source = LKS) for the 10 m and 50 m cases. As with the flow rate, there is a short transient with strong decompression cooling that settles back to increasing and then steady temperatures after about five minutes. A period of small oscillations occurs at around 6 min for the 10 m case. These are spurious artifacts arising from T2Well as the temperature approaches the lower limit of equation of state in the code. We use the near steady-state flow rate and LKS temperatures as input to TAMOC for steady-state water column transport modeling.

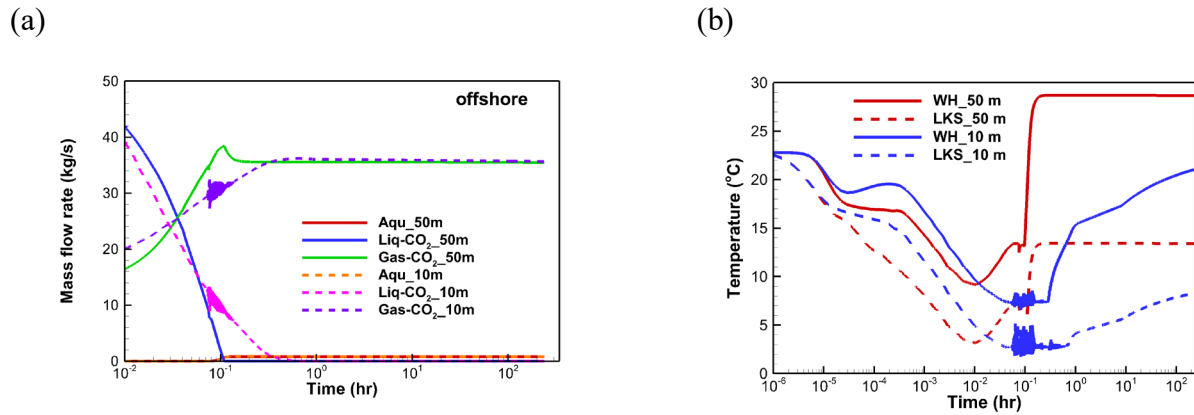


Figure 4. (a) Blowout flow rates versus time for the 10 and 50 m-depth cases, and (b) Temperature versus time for the 10 and 50 m-depth cases at the wellhead and at the hole (orifice).

## 2. Initial Bubble Sizes

The inputs to the bubble-size-estimation workflow for the scenario of the 50 m- and 10 m-deep blowouts from a 0.0508 m (2 inch) diameter hole near the well head are given in Table 3. As shown in Table 3, the CO<sub>2</sub> leakage rate and fluid properties as simulated by T2Well are quite similar for the two cases. The reason for this is that we have assumed hydrostatic pressure to set the reservoir pressure, making the  $\Delta P$  in the well the same for both cases. Specifically, ( $\Delta P_{50m} = P_{res} - P_{50m} = 30.03 - 0.60 \text{ MPa} = 29.43 \text{ MPa}$ , versus  $\Delta P_{10m} = P_{res} - P_{10m} = 29.63 - 0.20 = 29.43 \text{ MPa}$ ). Even if the reservoir and blowout depth location were not strictly correlated as we assumed, we note that the overpressures provided by the water column at the leak point on the seabed for a 50 m- or a 10 m-deep blowout location are not all that different relative to the overpressure in the well which is controlled by the deep reservoir. This first-order result that the subsurface part of CO<sub>2</sub> well blowouts will be very similar for offshore blowouts at depths between 10-50 m is similar to the result already reported<sup>22</sup> that onshore and near-offshore well blowouts will be similar insofar as blowout flow rate at the wellhead is concerned. The strong

differences between well blowouts at different depths offshore arises from transport in the water column as will be shown below.

We note that T2Well rigorously simulates the flow and PVT properties of CO<sub>2</sub> and water to avoid violating any physical limits on flow rate that could arise if the flow were to become choked at the orifice. Furthermore, for this case of CO<sub>2</sub> entering 23 °C shallow waters of the Texas Gulf Coast, it does not appear that CO<sub>2</sub>-hydrate will form around the orifice as the steady-state temperatures are too high and pressures are too low for hydrate stability (13.0 and 8.4 °C for the 50 and 10 m depth cases, respectively, and the ambient seawater pressures are only 0.598 and 0.202 MPa, respectively).

The similarity in CO<sub>2</sub> leakage conditions at different depths carries over to the estimation of bubble size and size distribution as shown Table 4. Note first that the volume-median bubble diameter ( $d_{50}$ ) is approximately 0.5 mm for both cases, which is quite small relative to the 3-8 mm bubble diameters observed at natural gas seeps<sup>19,58,59,60,61</sup>. The small bubble sizes in our simulations result from the large CO<sub>2</sub> blowout flow velocity and related turbulence. Smaller bubbles expose more surface area per unit volume and can be expected to dissolve faster. Note second that the value of  $l_M$ , the length scale for transition from jet to buoyant plume, is just over 2 m for both cases. This result suggests that for a leak in 10 m of water, transitioning of the flow from jet to buoyant plume will occur over one-fifth of the water column height ( $l_M = 2.12$  m) leaving only a short distance and rise time for buoyant plume flow where dissolution can occur. In contrast, there will be over 40 m of buoyant rise distance in the 50 m-deep leakage scenario during which the CO<sub>2</sub> buoyant plume will have time to slow down, spread out, and dissolve.

Table 3. Relevant output from T2Well and ambient seawater conditions for major CO<sub>2</sub> blowout for 50 m and 10 m water columns and 0.0508 m diameter hole.

Property	50 m depth	10 m depth	Units
Pressure of CO <sub>2</sub> at leakage orifice	4.0	3.8	MPa
Temperature at orifice	13.0	8.4	°C
CO <sub>2</sub> density at orifice	106.4	102.9	kg m <sup>-3</sup>
Diameter of orifice (hole)	0.0508	0.0508	m
Area of orifice (hole)	0.002027	0.002027	m <sup>2</sup>
CO <sub>2</sub> leakage flowrate	35.52	35.70	kg s <sup>-1</sup>
Mass-flux-based velocity ( $u_g$ )	162.3	172.6	m s <sup>-1</sup>
CO <sub>2</sub> surface tension	0.05 <sup>62</sup>	0.05 <sup>62</sup>	N m <sup>-1</sup>
Seawater temperature	22.8	22.8	°C
Ambient salinity	34.5	34.5	ppt
Seawater density	1025.0	1025.0	kg m <sup>-3</sup>
Seawater ambient current	0.15	0.15	m s <sup>-1</sup>

Table 4. Estimation of bubble sizes for the major CO<sub>2</sub> blowout for 50 m and 10 m water columns and 0.0508 m diameter hole.

Property	50 m depth	10 m depth	Units
$U_a$	52.29	54.69	m s <sup>-1</sup>
$M$	5.542	6.062	(m <sup>2</sup> s <sup>-2</sup> ) m <sup>2</sup>
$B$	2.892	3.088	m <sup>4</sup> s <sup>-3</sup>
$l_M$	2.12	2.20	m
$We_m$	1.236E+07	1.353E+07	-
$d_{50}/l_M$	2.39E-04	2.263E-04	-
$d_{50}$	5.075E-04	4.975E-04	m

Assuming the Rosin-Rammler distribution suggested by Wang et al.<sup>52</sup> and assuming a bubble-size range from 0.1-1.0 mm, we obtain the distributions shown in Table 5 and plotted in Figure 5 for the 50 and 10 m-deep scenarios. Note the similarities in bubble-size likelihoods for the most likely bubble sizes that cluster around the  $d_{50}$  value of 0.5 mm. In addition to larger surface area to volume ratio, small bubbles will tend to rise more slowly than larger bubbles providing more time for dissolution.

Table 5. Rosin-Rammler bubble size distribution for the 50 and 10 m-deep leakage scenarios with  $D = 0.0508$  m (2 inch hole).

Assumed bubble-size range (m)	50 m depth Cumulative likelihood $V(d)$	50 m depth Individual likelihood	10 m depth Cumulative likelihood $V(d)$	10 m depth Individual likelihood
1.00E-04	1.49E-04	1.49E-04	1.65E-04	1.65E-04
2.00E-04	5.45E-03	5.30E-03	6.05E-03	5.88E-03
3.00E-04	4.40E-02	3.86E-02	4.87E-02	4.27E-02
4.00E-04	1.82E-01	1.38E-01	2.00E-01	1.51E-01
5.00E-04*	4.73E-01	2.91E-01	5.09E-01	3.09E-01
6.00E-04	8.09E-01	3.36E-01	8.41E-01	3.31E-01
7.00E-04	9.75E-01	1.66E-01	9.83E-01	1.43E-01
8.00E-04	9.99E-01	2.44E-02	1.00E+00	1.64E-02
9.00E-04	1.00E+00	6.18E-04	1.00E+00	2.76E-04
1.00E-03	1.00E+00	1.20E-06	1.00E+00	2.71E-07

\*approximate  $d_{50}$

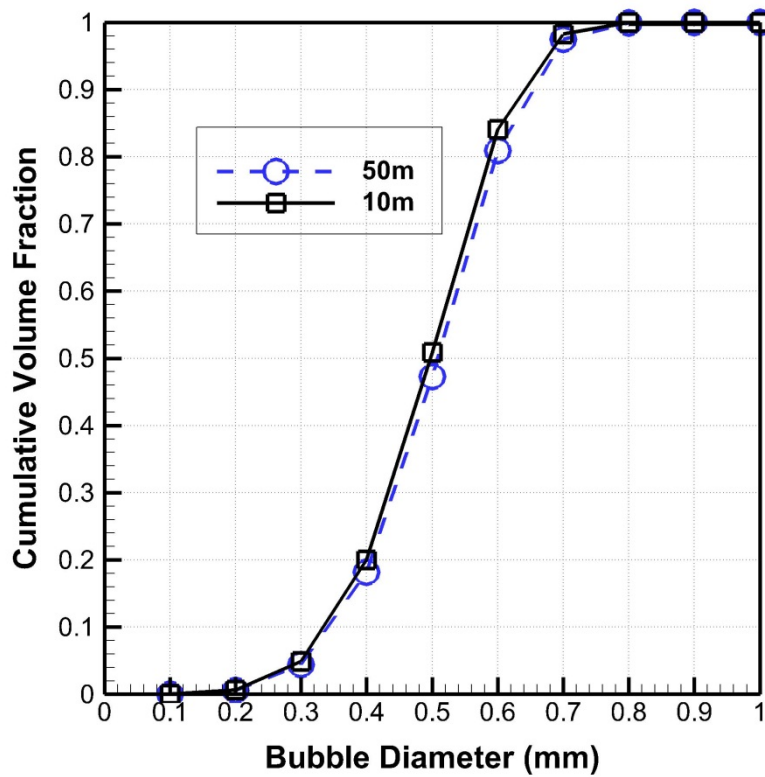


Figure 5. Cumulative volume fraction of bubble sizes for the 50 and 10 m-deep blowout cases.

### 3. Water Column Transport

Along with the bubble size distribution, the inputs to TAMOC include the orifice size and T2Well simulation outputs CO<sub>2</sub> leakage rate (kg/s) and temperature of the leaking CO<sub>2</sub>. Other inputs include the height of water column above the leak, and seawater pressure, temperature, salinity and ambient crossflow velocity. These properties are given in Table 3 for the 50 and 10 m-deep cases. Because of the similarity in leakage rate and derived quantities such as discharge velocity and bubble sizes for the 50 and 10 m-deep cases, we have interpolated a set of inputs for TAMOC for 20, 30, and 40 m-depth cases based on the 50 and 10 m-depth T2Well outputs. We present in Figure 6 the TAMOC outputs of the CO<sub>2</sub> flow rate emitted at the sea surface along with the fraction of CO<sub>2</sub> that dissolves in the water column for 10, 20, 30, 40, and 50 m-deep leakage scenarios. As shown, the CO<sub>2</sub> leakage flow rate is strongly attenuated for water column heights greater than 30 m, and almost all the leaked CO<sub>2</sub> dissolves in the water column for the 50 m-deep case. In contrast, almost all the leaked CO<sub>2</sub> at the sea floor in the 10 m-deep case is emitted into the atmosphere.

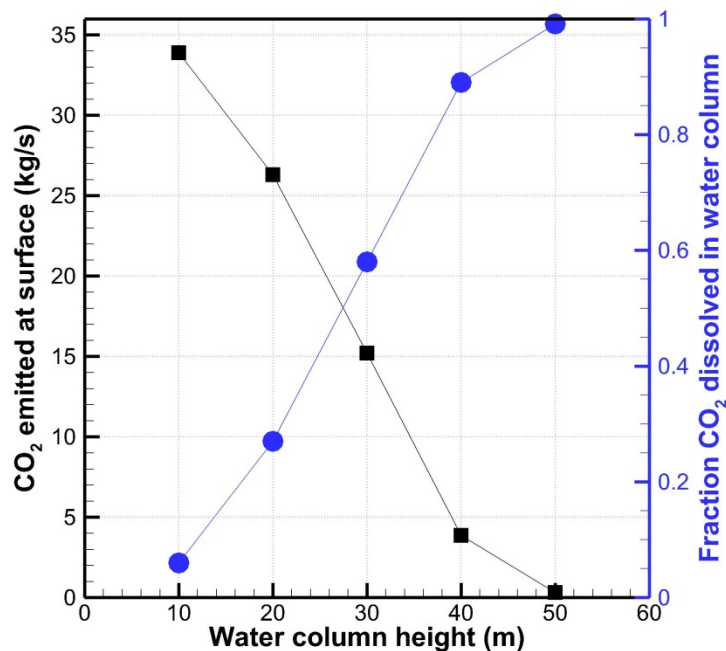


Figure 6. CO<sub>2</sub> flow rate at the sea surface (squares) and fraction of CO<sub>2</sub> dissolved in the water column (circles) as a function of water column height (depth of wellhead below sea surface).

TAMOC also calculates the travel times of the CO<sub>2</sub> blowout from leakage point to the sea surface and these are shown in Figure 7 for the five water column heights. As shown, the blowout travel time to the sea surface for the 10 m case is very short. The discharge velocity at the leakage point is 172.6 m/s, which if sustained throughout 10 m, would result in a travel time of 0.058 s. Instead, the travel time is 0.065 s, approximately 10% longer due probably to momentum transfer to ambient seawater. In contrast, the 50 m water column case more strongly retards the flow, and what small fraction of CO<sub>2</sub> that does not dissolve in the water column takes nearly five seconds to surface.

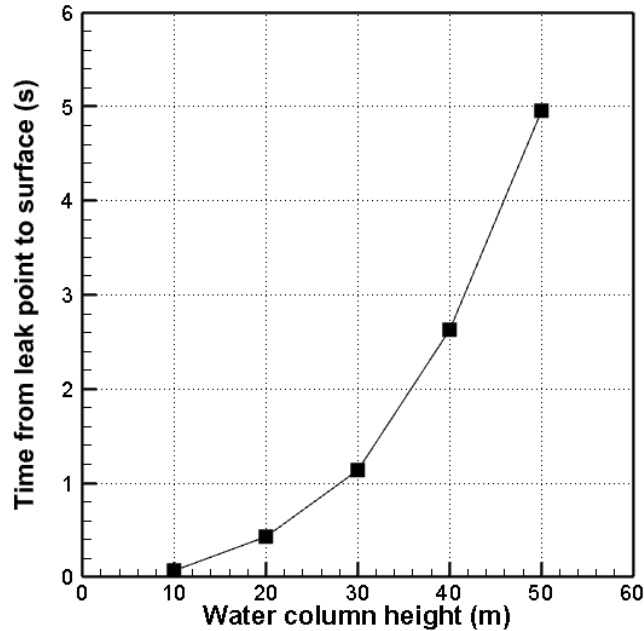


Figure 7. Travel time for the CO<sub>2</sub> blowout to arrive at the sea surface as a function of water column height (depth of wellhead leak below sea surface).

In Figure 8 we show TAMOC results for the deflection of the centerline of the CO<sub>2</sub> plume for the 10 and 50 m-depth cases, along with the plume lateral extent. With a nominal ambient flow of 0.15 m/s and a rise time of approximately 5 s, the plume is deflected approximately 0.75 m ( $0.15 \text{ m/s} \times 5 \text{ s} = 0.75 \text{ m}$ ) for the 50 m case, and a negligible amount for the 10 m case. The diameter of the plume in the 10 m case is about 3.2 m upon surfacing. The small fraction of the released CO<sub>2</sub> that surfaces in the 50 m case does so over a region approximately 15 m in diameter.

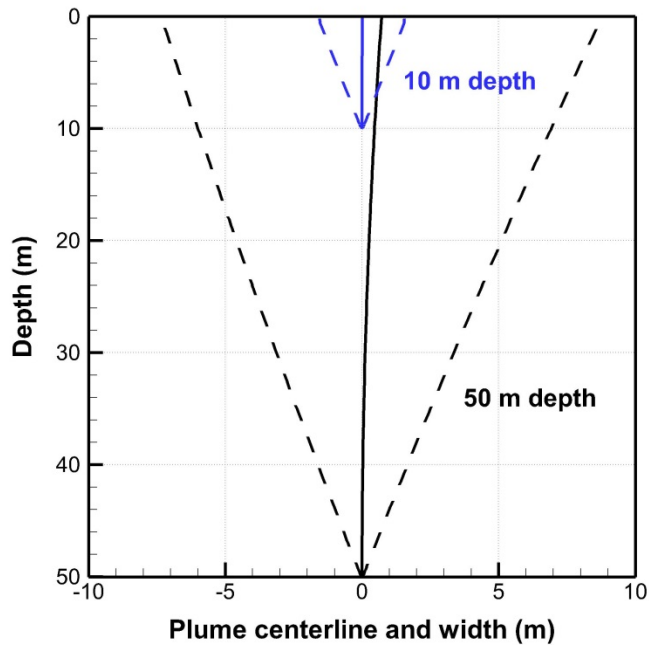


Figure 8. X-direction deflection of the centerline of the CO<sub>2</sub> plume (solid lines) due to the ambient cross flow and lateral extent of the plume (dashed lines) for the 10 and 50 m-depth cases.

In addition to the depth of the leak, another parameter that controls CO<sub>2</sub> transport is the size of the orifice (hole) through which the blowout occurs. We varied the diameter of the assumed circular hole (leakage source orifice) such that the area of the hole was 1/2, 1/5, 1/10, 1/50 and 1/100 the size of the base-case 0.0508 m diameter hole (2 inch-diameter hole). The main result of decreasing the hole size is to reduce the flow rate of the blowout simulated by T2Well as shown in Figure 9. T2Well and TAMOC results suggest that the CO<sub>2</sub> blowout flow rate and the emission at the sea surface are strongly affected by the hole size. The difference between the black and the blue curves indicates the degree of attenuation of CO<sub>2</sub> flow by the water column. As shown, and just as for the base-case 0.0508 m (2 inch) hole, the 10 m water column provides minimal attenuation of the leaking CO<sub>2</sub> regardless of hole size.

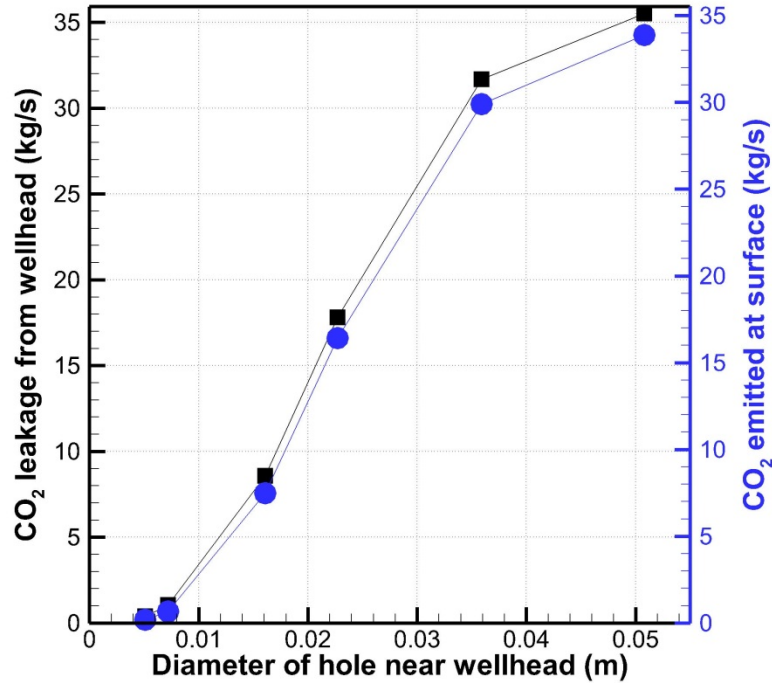


Figure 9. CO<sub>2</sub> blowout flow rate from the leak point (squares) and CO<sub>2</sub> flow rate of the surface emission (circles) as a function of the effective diameter of the hole near the wellhead for a water column depth of 10 m.

Although the results of Figure 9 are monotonic with hole size, the underlying processes are more interesting. We show in Figure 10 the CO<sub>2</sub> bubble size  $d_{50}$  calculated using the methods of Wang et al.<sup>52</sup> for the five varying-hole-size cases. As shown, a minimum bubble size occurs for intermediate-sized holes. As seen in Eq. 8, bubble size is a complicated non-linear function of the Weber number (exponent of -3/5) which varies with velocity squared and momentum length scale ( $l_M$ ), the latter of which is also in Eq. 8. In short, subtle variations in flow properties can combine to create unexpected variations in bubble sizes. We note also that CO<sub>2</sub> has strongly varying properties around its critical point and across the gas-liquid saturation line, regions of the phase diagram that are often encountered in CO<sub>2</sub> leakage and well-blowout situations, although not encountered in the present scenario.

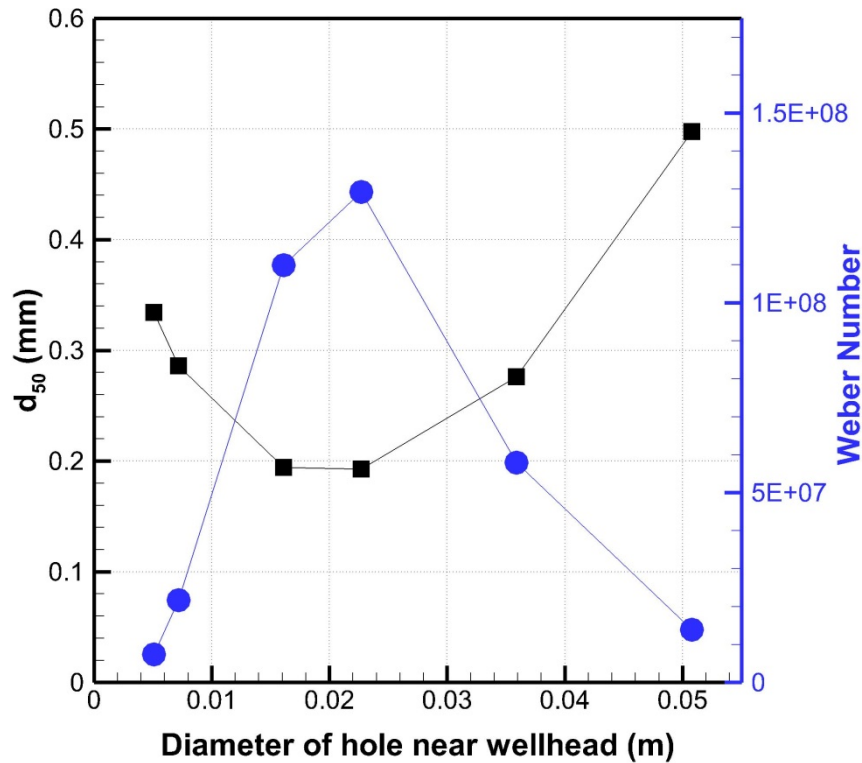


Figure 10.  $CO_2$  bubble size ( $d_{50}$ ) (squares) and Weber Number (circles) calculated by the methods of Wang et al. (2018) as a function of the diameter of the blowout hole near the wellhead.

### Conclusions and Discussion

We have carried out a modeling study of a generalized and hypothetical major blowout of an offshore  $CO_2$  well in shallow water. Although validation of the results presented here will have to await experiments or field observations of equivalent major blowout systems, based on the simulations carried out in this study, we offer the following conclusions:

- The water column will provide strong attenuation of the  $CO_2$  surface emission provided the blowout occurs in more than about 50 m of water (> 165 ft).
- In 30 m (> 100 ft) or more of water, less than one-half of the blowout  $CO_2$  flow will surface, and in 50 m or more, only a small percentage of the leaked  $CO_2$  will reach the surface.
- Major blowouts in shallow water (e.g., 10 m or less) are not attenuated appreciably by the water column.

- The CO<sub>2</sub> blowout flow rate and therefore the surface emission is strongly controlled by the size of the leakage orifice, while attenuation (fraction surfacing) is controlled by water column height.

Some secondary conclusions of the study are

- The length scale for the transition from jet to buoyant plume of CO<sub>2</sub> leaking out of the orifice into ambient seawater is approximately 2 m at depths of 10-50 m.
- The blowout flow rate into shallow waters (10-50 m depth) is not very sensitive to water column height because reservoir pressure is much larger than seafloor pressure for shallow offshore wells.
- Bubble sizes for vigorous CO<sub>2</sub> blowouts are predicted to be quite small (~0.5 mm) which enhances dissolution in the water column.
- Processes attending major CO<sub>2</sub> blowouts of near offshore wells into the water column are not strongly coupled and modeling of these processes does not have to be fully coupled.
- On the other hand, modeling of major blowouts always requires coupling between flow in the reservoir and the well.

The primary result that seawater is effective at attenuating offshore (subsea) CO<sub>2</sub> blowouts is consistent with what we know about attenuation of natural gas blowouts and seeps<sup>63</sup> and the relatively larger solubility of CO<sub>2</sub> in seawater relative to CH<sub>4</sub>. Specifically, natural gas associated with oil well blowouts is well-known to dissolve in the water column for cases of deep-water blowouts such as the 2010 Macondo well blowout<sup>64,65</sup> and from theoretical, modeling, and experimental studies<sup>10,4,66</sup>. When one considers that CO<sub>2</sub> solubility in water is approximately 25 times larger than that of CH<sub>4</sub><sup>67</sup> and this factor carries over to seawater<sup>68,69</sup>, the strong attenuation of CO<sub>2</sub> blowouts is not surprising.

Another factor favoring dissolution in the water column is the small bubble size predicted to occur for high-flow-rate CO<sub>2</sub> blowouts which creates a high surface area to volume ratio favoring fast dissolution<sup>10</sup>. We can also demonstrate this by looking at Eq. 10, which we can rearrange to roughly approximate the time it takes for a CO<sub>2</sub> bubble to dissolve

$$\Delta t = \frac{\Delta m_i}{A_b \beta_i (C_{s,i} - C_i^{eq})} \quad (11)$$

where the approximate mass transfer coefficient for CO<sub>2</sub> in water is  $1 \times 10^{-4}$  m/s for bubbles of diameter 0.5 mm as estimated by correlations for contaminated (i.e., dirty) bubbles<sup>54</sup>. If we look at the median size bubble (0.5 mm) and assume the ambient CO<sub>2</sub> concentration ( $C_i^{eq}$ ) is negligible relative to the CO<sub>2</sub> concentration in the seawater in the seawater skin of the gas-bubble interface ( $C_{s,i}$ ) which is equal to the solubility of CO<sub>2</sub> in seawater assuming pure CO<sub>2</sub> gas fills the bubble at the local water-column pressure ( $C_{s,i} = 2.62$  kg CO<sub>2</sub>/m<sup>3</sup> seawater for the 10 m-

deep blowout and  $C_{s,i} = 7.83 \text{ kg CO}_2/\text{m}^3$  seawater for the 50 m-deep blowout using published solubility values<sup>68</sup>), we find the time to dissolve the bubble is 1.14 s. It turns out this time to dissolve is independent of depth over the 10-50 m depth range because both the mass of  $\text{CO}_2$  in the bubble (numerator in Eq. 11) and the dissolved  $\text{CO}_2$  at the bubble interface (in the denominator in Eq. 11) scale almost linearly with depth at shallow depths (more mass in bubble at larger depth because gas density is higher, but also higher solubility in seawater at greater depth). In deep-water conditions, non-ideal effects of  $\text{CO}_2$  would likely arise altering this balance between density and solubility increase.

Although roughly independent of depth, the time to dissolve the bubble is strongly dependent on the surface area to volume ratio as shown in Eq. 11 where area is in the denominator and volume is implicit in the mass term in the numerator. And this effect of surface area to volume strictly affects only the dissolution rate, whereas bubble rise time also comes into play when considering complete absorption of bubbles by seawater because small bubbles rise more slowly than large bubbles.. Looking also at the depth of the gas release from Fig. 7 and related text, we note the rise time for the 10 m-deep blowout is 0.065 s, too fast for significant bubble dissolution to occur, while the rise time for the 50 m-deep blowout is five seconds, enough time for the 0.5 mm bubbles (and the 1 mm bubbles which are estimated by this analysis to dissolve in approximately 2.28 s) to dissolve leading to nearly full absorption of  $\text{CO}_2$  into the seawater. Note that this simple analysis overestimates the dissolution rate because the plume seawater concentration ( $C_i^{eq}$ ) in TAMOC is not zero but rather is calculated as the ratio of the simulated mass of  $\text{CO}_2$  lost from bubbles by dissolution to the corresponding simulated plume seawater volume.

Although we do not observe hydrate stability conditions for the scenario we chose, T2Well results show strong decompression cooling and associated low temperatures. The fact is that other blowout scenarios, even in near-offshore Gulf of Mexico sites, could lead to sub-zero temperatures in the well or near the orifice and possibility of ice and/or  $\text{CO}_2$  hydrate formation. From a risk-assessment perspective where emission of  $\text{CO}_2$  at the sea surface is the main risk driver, formation of ice or hydrate may serve to reduce  $\text{CO}_2$  blowout rates and reduce risk, although specific analyses of hydrate scenarios are needed to assess this further.

## Nomenclature

Symbols	Description	Units
$A$	Area of the orifice	$\text{m}^2$
$A_g$	Area of the orifice over which gas is leaking	$\text{m}^2$
$A_b$	Surface area of bubble	$\text{m}^2$
$b_0$	Buoyant momentum flux	$\text{kg m s}^{-3}$
$B$	Buoyant momentum flux normalized by seawater density	$\text{m}^4 \text{s}^{-3}$
$C_i^{eq}$	Equilibrium aqueous concentration of component $i$ in seawater	$\text{kg m}^{-3}$
$C_{s,i}$	Aqueous concentration of component $i$ in seawater at the bubble-seawater interface	$\text{kg m}^{-3}$
$d_{50}$	Volumetric median diameter	m or mm
$D$	Diameter of the orifice	m or inch
$k_{50}$	Empirical constant in Rosin-Rammler equation	-
$l_M$	Length scale for transition from jet to buoyant plume	m
$m_0$	Kinematic momentum flux	$\text{kg (m}^{-1} \text{s}^{-2}) \text{m}^2$
$m_i$	mass of component $i$	kg
$M$	Kinematic momentum flux normalized by seawater density	$(\text{m}^2 \text{s}^{-2}) \text{m}^2$
$t$	time	s
$u_g$	Velocity of gas	$\text{m s}^{-1}$
$U_a$	Velocity of mixture of gas and ambient seawater	$\text{m s}^{-1}$
$V(d)$	Volumetric bubble-size distribution	-
$We_m$	Weber number	-
Greek Symbols		
$\alpha$	Exponent in Rosin-Rammler bubble size distribution	-
$\beta$	Mass transfer coefficient	$\text{m s}^{-1}$
$\rho_g$	Density of gas	$\text{kg m}^{-3}$
$\rho_a$	Density of ambient seawater	$\text{kg m}^{-3}$
$\sigma$	Surface tension of $\text{CO}_2$ in seawater	$\text{N m}^{-1}$

## Acknowledgments

We thank Scott Socolofsky (Texas A&M University) and Jonas Gros (GEOMAR Helmholtz Centre for Ocean Research Kiel) for advice and assistance with using TAMOC, and two anonymous reviewers whose comments led to significant improvements in both content and presentation. This work was supported by the GoMCarb Project funded by the Assistant Secretary for Fossil Energy (DOE), Office of Clean Coal and Carbon Management, through the National Energy Technology Laboratory (NETL), and by Lawrence Berkeley National Laboratory under Department of Energy Contract No. DE-AC02-05CH11231.

## References

1. Metz, B., Davidson, O., De Coninck, H., Loos, M. and Meyer, L., 2005. *IPCC special report on carbon dioxide capture and storage*. Intergovernmental Panel on Climate Change, Geneva (Switzerland). Working Group III.
2. McNutt, M.K., Camilli, R., Crone, T.J., Guthrie, G.D., Hsieh, P.A., Ryerson, T.B., Savas, O. and Shaffer, F., 2012. Review of flow rate estimates of the Deepwater Horizon oil spill. *Proceedings of the National Academy of Sciences*, 109(50), pp.20260-20267.
3. Conley, S., Franco, G., Faloona, I., Blake, D.R., Peischl, J. and Ryerson, T.B., 2016. Methane emissions from the 2015 Aliso Canyon blowout in Los Angeles, CA. *Science*, 351(6279), pp.1317-1320.
4. Xinhong, L., Guoming, C., Renren, Z., Hongwei, Z., and Jianmin, F., 2018. Simulation and assessment of underwater gas release and dispersion from subsea gas pipelines leak. *Process Safety and Environmental Protection*, 119, 46-57.
5. Blackford, J.C., Jones, N., Proctor, R. and Holt, J., 2008. Regional scale impacts of distinct CO<sub>2</sub> additions in the North Sea. *Marine Pollution Bulletin*, 56(8), pp.1461-1468.
6. Blackford, J., Jones, N., Proctor, R., Holt, J., Widdicombe, S., Lowe, D. and Rees, A., 2009. An initial assessment of the potential environmental impact of CO<sub>2</sub> escape from marine carbon capture and storage systems. *Proceedings of the Institution of Mechanical Engineers, Part A: Journal of Power and Energy*, 223(3), pp.269-280.
7. Taylor, P., Stahl, H., Vardy, M.E., Bull, J.M., Akhurst, M., Hauton, C., James, R.H., Lichtschlag, A., Long, D., Aleynik, D. and Toberman, M., 2015. A novel sub-seabed CO<sub>2</sub> release experiment informing monitoring and impact assessment for geological carbon storage. *International Journal of Greenhouse Gas Control*, 38, pp.3-17.
8. Gasda, S.E., Bachu, S. and Celia, M.A., 2004. Spatial characterization of the location of potentially leaky wells penetrating a deep saline aquifer in a mature sedimentary basin. *Environmental Geology*, 46(6-7), pp.707-720.
9. Nordbotten, J.M., Celia, M.A. and Bachu, S., 2004. Analytical solutions for leakage rates through abandoned wells. *Water Resources Research*, 40(4).
10. Olsen, J.E., and Skjetne, P., 2016. Current understanding of subsea gas release: A review. *The Canadian Journal of Chemical Engineering*, 94(2), 209-219.
11. Jordan, P.D. and Benson, S.M., 2009. Well blowout rates and consequences in California Oil and Gas District 4 from 1991 to 2005: implications for geological storage of carbon dioxide. *Environmental Geology*, 57(5), pp.1103-1123.

12. Porse, S.L., Wade, S., and Hovorka, S.D., 2014. Can we treat CO<sub>2</sub> well blowouts like routine plumbing problems? A study of the incidence, impact, and perception of loss of well control. *Energy Procedia*, 63, 7149-7161.
13. Meckel, T. A., Trevino, R., & Hovorka, S. D., 2017. Offshore CO<sub>2</sub> storage resource assessment of the northern Gulf of Mexico. *Energy Procedia*, 114, 4728-4734.
14. Brock, W.R. and Bryan, L.A., 1989, January. Summary results of CO<sub>2</sub>-EOR field tests, 1972-1987. In Low permeability reservoirs symposium. *Society of Petroleum Engineers*.
15. Lynch, R.D., McBride, E.J., Perkins, T.K. and Wiley, M.E., 1985. Dynamic kill of an uncontrolled CO<sub>2</sub> well. *Journal of Petroleum Technology*, 37(07), pp.1-267.
16. Newswest9, Oil Well Blowout Reported in Gaines County, Evacuations in Effect, December 8, 2015, <http://www.newswest9.com/story/30695088/oil-well-blowout-reported-in-gaines-county/>
17. Ardelan, M.V., Steinnes, E., Lierhagen, S. and Linde, S.O., 2009. Effects of experimental CO<sub>2</sub> leakage on solubility and transport of seven trace metals in seawater and sediment. *Science of the Total Environment*, 407(24), pp.6255-6266.
18. Blackford, J., Stahl, H., Bull, J.M., Bergès, B.J., Cevatoglu, M., Lichtschlag, A., Connelly, D., James, R.H., Kita, J., Long, D. and Naylor, M., 2014. Detection and impacts of leakage from sub-seafloor deep geological carbon dioxide storage. *Nature Climate Change*, 4(11), p.1011.
19. Gros, J., Schmidt, M., Dale, A.W., Linke, P., Vielstädte, L., Bigalke, N., Haeckel, M., Wallmann, K. and Sommer, S., 2019. Simulating and Quantifying Multiple Natural Subsea CO<sub>2</sub> Seeps at Panarea Island (Aeolian Islands, Italy) as a Proxy for Potential Leakage from Subseabed Carbon Storage Sites. *Environmental Science & Technology*.
20. Phelps, J.J., Blackford, J.C., Holt, J.T., and Polton, J.A., 2015. Modelling large-scale CO<sub>2</sub> leakages in the North Sea. *International Journal of Greenhouse Gas Control*, 38, 210-220.
21. Pan, L., Oldenburg, C.M., Pruess, K., and Wu, Y.S., 2011. Transient CO<sub>2</sub> leakage and injection in wellbore-reservoir systems for geologic carbon sequestration. *Greenhouse Gases: Science and Technology*, 1(4), 335-350.
22. Oldenburg, C.M., and Pan, L., 2019. Simulation study comparing offshore versus onshore CO<sub>2</sub> well blowouts, Offshore Technology Conference, OTC-29461-MS, May 6-10, 2019, Houston, TX.
23. Cloete, S., Olsen, J.E. and Skjetne, P., 2009. CFD modeling of plume and free surface behavior resulting from a sub-sea gas release. *Applied Ocean Research*, 31(3), pp.220-225.
24. Engebretsen, T., Northug, T., Sjøen, K. and Fanneløp, T.K., 1997, January. Surface flow and gas dispersion from a subsea release of natural gas. In The Seventh International Offshore and Polar Engineering Conference. International Society of Offshore and Polar Engineers.

25. Fannelop, T. and Sjoen, K., 1980, January. Hydrodynamics of underwater blowouts. *In 18th Aerospace Sciences Meeting* (p. 219).
26. Milgram, J. H., 1983. Mean flow in round bubble plumes. *Journal of Fluid Mechanics*, 133, 345-376.
27. Yapa, P. D., & Zheng, L. (1997). Modelling oil and gas releases from deep water: A review. *Spill Science & Technology Bulletin*, 4(4), 189-198.
28. Zheng, L., Yapa, P. D., and Chen, F., 2003. A model for simulating deepwater oil and gas blowouts-Part I: Theory and model formulation. *Journal of Hydraulic Research*, 41(4), 339-351.
29. Johansen, Ø., 2003. Development and verification of deep-water blowout models. *Marine Pollution Bulletin*, 47(9-12), pp.360-368.
30. Spaulding, M., Li, Z., Mendelsohn, D., Crowley, D., French-McCay, D. and Bird, A., 2017. Application of an integrated blowout model system, OILMAP DEEP, to the deepwater Horizon (DWH) Spill. *Marine Pollution Bulletin*, 120(1-2), pp.37-50.
31. Socolofsky, S.A., Dissanayake, A.L., Jun, I., Gros, J., Arey, J.S. and Reddy, C.M., 2015. Texas A&M Oilspill Calculator (TAMOC): Modeling Suite for Subsea Spills. In *Proceedings of the Thirty-Eighth AMOP Technical Seminar* (Environment Canada, Ottawa) (pp. 153-168).
32. Gros, J., Reddy, C.M., Nelson, R.K., Socolofsky, S.A. and Arey, J.S., 2016. Simulating gas-liquid-water partitioning and fluid properties of petroleum under pressure: implications for deep-sea blowouts. *Environmental Science & Technology*, 50(14), pp.7397-7408.
33. Gros, J., Socolofsky, S.A., Dissanayake, A.L., Jun, I., Zhao, L., Boufadel, M.C., Reddy, C.M. and Arey, J.S., 2017. Petroleum dynamics in the sea and influence of subsea dispersant injection during Deepwater Horizon. *Proceedings of the National Academy of Sciences*, 114(38), pp.10065-10070.
34. Dissanayake, A.L., Gros, J. and Socolofsky, S.A., 2018. Integral models for bubble, droplet, and multiphase plume dynamics in stratification and crossflow. *Environmental Fluid Mechanics*, 18(5), pp.1167-1202.
35. Gasda, S.E., Nordbotten, J.M. and Celia, M.A., 2012. Application of simplified models to CO<sub>2</sub> migration and immobilization in large-scale geological systems. *International Journal of Greenhouse Gas Control*, 9, pp.72-84.
36. Andrew, J.C., Haszeldine, R.S. and Nazarian, B., 2015. The Sleipner CO<sub>2</sub> storage site: using a basin model to understand reservoir simulations of plume dynamics. *First Break*, 33(6), pp.61-68.
37. Lindeberg, E., Bergmo, P., Torsæter, M. and Grimstad, A.A., 2017. Aliso Canyon leakage as an analogue for worst case CO<sub>2</sub> leakage and quantification of acceptable storage loss. *Energy Procedia*, 114, pp.4279-4286.

38. Pan, L., 2011. "T2Well/ECO<sub>2</sub>N version 1.0: multiphase and non-isothermal model for coupled wellbore-reservoir flow of carbon dioxide and variable salinity water." Lawrence Berkeley National Laboratory *Report LBNL-4291e*.
39. Pan, L., and Oldenburg, C.M., 2014. T2Well—an integrated wellbore–reservoir simulator. *Computers & Geosciences*, 65, 46-55.
40. Pan, L., Spycher, N., Doughty, C., and Pruess, K., 2015. ECO<sub>2</sub>N V2. 0: A TOUGH2 fluid property module for mixtures of water, NaCl, and CO<sub>2</sub>. *Scientific report LBNL-6930E*.
41. Oldenburg, C.M., Freifeld, B.M., Pruess, K., Pan, L., Finsterle, S., and Moridis, G.J., 2012. Numerical simulations of the Macondo well blowout reveal strong control of oil flow by reservoir permeability and exsolution of gas. *Proceedings of the National Academy of Sciences*, 109(50), 20254-20259.
42. Pan, L., Oldenburg, C.M., Freifeld, B.M., and Jordan, P. D., 2018. Modeling the Aliso Canyon underground gas storage well blowout and kill operations using the coupled well-reservoir simulator T2Well. *Journal of Petroleum Science and Engineering*, 161, 158-174.
43. Gros, J., Dissanayake, A.L., Daniels, M.M., Barker, C.H., Lehr, W. and Socolofsky, S.A., 2018. Oil spill modeling in deep waters: Estimation of pseudo-component properties for cubic equations of state from distillation data. *Marine Pollution Bulletin*, 137, pp.627-637.
44. Asaeda, T. and Imberger, J., 1993. Structure of bubble plumes in linearly stratified environments. *Journal of Fluid Mechanics*, 249, pp.35-57.
45. Socolofsky, S.A., Bhaumik, T. and Seol, D.G., 2008. Double-plume integral models for near-field mixing in multiphase plumes. *Journal of Hydraulic Engineering*, 134(6), pp.772-783.
46. McGinnis, D.F., Lorke, A., Wüest, A., Stöckli, A. and Little, J.C., 2004. Interaction between a bubble plume and the near field in a stratified lake. *Water Resources Research*, 40(10).
47. McGinnis, D.F., Greinert, J., Artemov, Y., Beaubien, S.E. and Wüest, A.N.D.A., 2006. Fate of rising methane bubbles in stratified waters: How much methane reaches the atmosphere? *Journal of Geophysical Research: Oceans*, 111(C9).
48. Fischer, H.B., List, J.E., Koh, C.R., Imberger, J. and Brooks, N.H., 2013. *Mixing in inland and coastal waters*. Elsevier.
49. Wüest, A., Brooks, N. H., and Imboden, D. M., 1992. Bubble plume modeling for lake restoration. *Water Resources Research*, 28(12), 3235-3250.
50. Jirka, G.H., 2004. Integral model for turbulent buoyant jets in unbounded stratified flows. Part I: Single round jet. *Environmental Fluid Mechanics*, 4(1), pp.1-56.

51. Leonte, M., Wang, B., Socolofsky, S.A., Mau, S., Breier, J.A. and Kessler, J.D., 2018. Using Carbon Isotope Fractionation to Constrain the Extent of Methane Dissolution Into the Water Column Surrounding a Natural Hydrocarbon Gas Seep in the Northern Gulf of Mexico. *Geochemistry, Geophysics, Geosystems*, 19(11), pp.4459-4475.
52. Wang, B., Socolofsky, S.A., Lai, C.C., Adams, E.E., and Boufadel, M.C., 2018. Behavior and dynamics of bubble breakup in gas pipeline leaks and accidental subsea oil well blowouts. *Marine pollution bulletin*, 131, 72-86.
53. Clift, R., Grace, J.R. and Weber, M.E., 2005. *Bubbles, drops, and particles*. Courier Corporation.
54. Olsen, J.E., Dunnebier, D., Davies, E., Skjetne, P. and Morud, J., 2017. Mass transfer between bubbles and seawater. *Chemical Engineering Science*, 161, pp.308-315.
55. Van Genuchten, M. T., 1980. A closed-form equation for predicting the hydraulic conductivity of unsaturated soils 1. *Soil Science Society of America Journal*, 44(5), 892-898.
56. Ramey H.J. Jr, 1962. Wellbore heat transmission. *J Petrol Technol* 225:427–435.
57. Corey, A.T., 1954. The interrelation between gas and oil relative permeabilities. *Producers monthly*, 19(1), pp.38-41.
58. Römer, M., Sahling, H., Pape, T., Bohrmann, G. and Spieß, V., 2012. Quantification of gas bubble emissions from submarine hydrocarbon seeps at the Makran continental margin (offshore Pakistan). *Journal of Geophysical Research: Oceans*, 117(C10).
59. Sellami, N., Dewar, M., Stahl, H. and Chen, B., 2015. Dynamics of rising CO<sub>2</sub> bubble plumes in the QICS field experiment: Part 1–The experiment. *International Journal of Greenhouse Gas Control*, 38, pp.44-51.
60. Wang, B. and Socolofsky, S.A., 2015. A deep-sea, high-speed, stereoscopic imaging system for in situ measurement of natural seep bubble and droplet characteristics. *Deep Sea Research Part I: Oceanographic Research Papers*, 104, pp.134-148.
61. Vielstädte, L., Karstens, J., Haeckel, M., Schmidt, M., Linke, P., Reimann, S., Liebetrau, V., McGinnis, D.F. and Wallmann, K., 2015. Quantification of methane emissions at abandoned gas wells in the Central North Sea. *Marine and Petroleum Geology*, 68, pp.848-860.
62. Kvamme, B., Kuznetsova, T., Hebach, A., Oberhof, A. and Lunde, E., 2007. Measurements and modelling of interfacial tension for water+ carbon dioxide systems at elevated pressures. *Computational Materials Science*, 38(3), pp.506-513.
63. McGinnis, D.F., Schmidt, M., DelSontro, T., Themann, S., Rovelli, L., Reitz, A. and Linke, P., 2011. Discovery of a natural CO<sub>2</sub> seep in the German North Sea: Implications for shallow dissolved gas and seep detection. *Journal of Geophysical Research: Oceans*, 116(C3).

64. Reddy, C.M., Arey, J.S., Seewald, J.S., Sylva, S.P., Lemkau, K.L., Nelson, R.K., Carmichael, C.A., McIntyre, C.P., Fenwick, J., Ventura, G.T. and Van Mooy, B.A., 2012. Composition and fate of gas and oil released to the water column during the Deepwater Horizon oil spill. *Proceedings of the National Academy of Sciences*, 109(50), pp.20229-20234.
65. Ryerson, T.B., Camilli, R., Kessler, J.D., Kujawinski, E.B., Reddy, C.M., Valentine, D.L., Atlas, E., Blake, D.R., De Gouw, J., Meinardi, S. and Parrish, D.D., 2012. Chemical data quantify Deepwater Horizon hydrocarbon flow rate and environmental distribution. *Proceedings of the National Academy of Sciences*, 109(50), pp.20246-20253.
66. Vielstädte, L., Linke, P., Schmidt, M., Sommer, S., Haeckel, M., Braack, M. and Wallmann, K., 2019. Footprint and detectability of a well leaking CO<sub>2</sub> in the Central North Sea: Implications from a field experiment and numerical modelling. *International Journal of Greenhouse Gas Control*, 84, pp.190-203.
67. Oldenburg, C.M., and Lewicki, J.L., 2006. On leakage and seepage of CO<sub>2</sub> from geologic storage sites into surface water. *Environmental Geology*, 50(5), 691-705.
68. Weiss, R., 1974. Carbon dioxide in water and seawater: the solubility of a non-ideal gas. *Marine chemistry*, 2(3), pp.203-215.
69. Yamamoto, S., Alcauskas, J.B. and Crozier, T.E., 1976. Solubility of methane in distilled water and seawater. *Journal of Chemical and Engineering Data*, 21(1), pp.78-80.